Human Molecular Genetics, 2005, Vol. 14, No. 11 ***1515–1528***
doi:10.1093/hmg/ddi160
Advance Access published on April 20, 2005

Genetic models show that parathyroid hormone and 1,25-dihydroxyvitamin D_3 play distinct and synergistic roles in postnatal mineral ion homeostasis and skeletal development

Yingben Xue[1], Andrew C. Karaplis[2], Geoffrey N. Hendy[1], David Goltzman[1] and Dengshun Miao[1,*]

[1]Calcium Research Laboratory, McGill University Health Centre and Department of Medicine, McGill University, Montreal, Quebec H3A 1A1, Canada and [2]Lady Davis Research Institute, Sir Mortimer B. Davis—Jewish General Hospital and Department of Medicine McGill University, Montreal, Quebec H3T 1E2, Canada

Received February 19, 2005; Revised and Accepted April 11, 2005

In humans, loss-of-function mutations in parathyroid hormone (PTH) and 25-hydroxyvitamin D_3-1α-hydroxylase [1α(OH)ase] genes lead to isolated hypoparathyroidism and vitamin D-dependent rickets type I, respectively. To better understand the relative contributions of PTH and 1,25-dihydroxyvitamin D_3 [$1,25(OH)_2D_3$] to skeletal and calcium homeostasis, we compared mice with targeted disruption of the PTH or 1α(OH)ase genes to the double null mutants. Although $PTH^{-/-}$ and $1\alpha(OH)ase^{-/-}$ mice displayed only moderate hypocalcemia, $PTH^{-/-}1\alpha(OH)ase^{-/-}$ mice died of tetany with severe hypocalcemia by 3 weeks of age. At 2 weeks, $PTH^{-/-}$ mice exhibited only minimal dysmorphic changes, whereas $1\alpha(OH)ase^{-/-}$ mice displayed epiphyseal dysgenesis which was most severe in the double mutants. Although reduced osteoblastic bone formation was seen in both mutants, PTH deficiency caused only a slight reduction in long bone length but a marked reduction in trabecular bone volume, whereas 1α(OH)ase ablation caused a smaller reduction in trabecular bone volume but a significant decrease in bone length. The results therefore show that PTH plays a predominant role in appositional bone growth, whereas $1,25(OH)_2D_3$ acts predominantly on endochondral bone formation. Although PTH and $1,25(OH)_2D_3$ independently, but not additively, regulate osteoclastic bone resorption, they do affect the renal calcium transport pathway cooperatively. Consequently, PTH and $1,25(OH)_2D_3$ exhibit discrete and collaborative roles in modulating skeletal and calcium homeostasis and loss of the renal component of calcium conservation might be the major factor contributing to the lethal hypocalcemia in double mutants.

INTRODUCTION

The vitamin D-parathyroid hormone (PTH) axis plays a central role in calcium and phosphate homeostasis and is essential for skeletal development and mineralization. PTH and 1,25-dihydroxyvitamin D_3 [$1,25(OH)_2D_3$] directly affect calcium homeostasis and each exerts important regulatory effects on the other. PTH stimulates the production of $1,25(OH)_2D_3$ by activating the renal 25-hydroxyvitamin D-1α-hydroxylase [1α(OH)ase] (1,2) and $1,25(OH)_2D_3$ which in turn suppresses the production of PTH (3,4) and controls parathyroid cell growth (5). $1,25(OH)_2D_3$ suppression of PTH synthesis occurs through negative regulation of PTH gene transcription by a $1,25(OH)_2D_3$-vitamin D receptor (VDR)/retinoid X receptor (RXR) complex (6) in the parathyroid cell (7). Vitamin D deficiency, both directly and by inducing hypocalcemia, also causes parathyroid hyperplasia.

Loss-of-function mutations in the PTH gene have been described in isolated forms of hypoparathyroidism (8–10), leading to decreased PTH secretion. Thus, cases of familial

*To whom correspondence should be addressed at: Calcium Research Laboratory, Rm: H4.67, Royal Victoria Hospital, 687 Pine Avenue West, Montreal, Quebec H3A 1A1, Canada. Tel: +1 5148431632; Fax: +1 5148431712; Email: dengshun.miao@mcgill.ca

© *The Author 2005. Published by Oxford University Press. All rights reserved.*
For Permissions, please email: journals.permissions@oupjournals.org

Downloaded from https://academic.oup.com/hmg/article/14/11/1515/605493 by guest on 20 April 2024

hypoparathyroidism have been reported, in which a T–C mutation in exon II of the PTH gene has occurred resulting in a cysteine to arginine substitution at position 18 of the signal peptide and in which a G–C mutation at the first nucleotide of intron II has occurred resulting in exon skipping and loss of exon II. In both cases, PTH insertion into the secretory pathway is impaired. Although reduced circulating PTH occurs with resultant hypocalcemia, isolated hypoparathyroidism is rarely lethal.

Loss-of-function mutations in the 1α(OH)ase gene have also been described leading to diminished production of $1,25(OH)_2D_3$ and the autosomal recessive disorder, vitamin D-dependent rickets type I (also called pseudovitamin D deficiency rickets) (11). Although hypocalcemia and skeletal alterations occur, this defect is also not lethal.

We have previously reported a mouse model deficient in PTH by targeting the *Pth* gene in embryonic stem cells. Although adult *Pth*-null mice develop hypocalcemia, hyperphosphatemia and low circulating $1,25(OH)_2D_3$ levels consistent with primary hypoparathyroidism (12), this phenotype is not lethal. We (13) and others (14) have also previously reported a mouse model deficient in $1,25(OH)_2D$ by targeted ablation of the 1α(OH)ase gene ($1\alpha(OH)ase^{-/-}$). After being weaned, mice, fed a diet of regular mouse chow, developed secondary hyperparathyroidism, retarded growth and the skeletal abnormalities characteristic of rickets. These abnormalities mimic those described in vitamin D-dependent rickets type I (15,16). This mouse phenotype is also not lethal.

Therefore, despite the fact that $1,25(OH)_2D_3$ and PTH are the most important regulators of calcium homeostasis, mice with targeted deletion of either PTH or 1α(OH)ase are viable and exhibit only moderate hypocalcemia (12,13). The viability of animals with 1α(OH)ase gene ablation might be the result of compensation by PTH to maintain a sufficiently high serum calcium level for survival of the $1\alpha(OH)ase^{-/-}$ mice (13). However, in the case of animals with PTH ablation, serum $1,25(OH)_2D_3$ levels are significantly reduced at least in the adult. It is unknown how postnatal PTH deficient mice maintain serum at sufficient calcium levels to survive and whether animals lacking both $1,25(OH)_2D_3$ and PTH genes are viable due to compensatory actions of other factors.

Both $1,25(OH)_2D_3$ and PTH exert catabolic and anabolic actions on bone and both are used clinically for the management of osteoporosis; however, the mechanisms of the interaction between $1,25(OH)_2D_3$ and PTH in bone remodeling are not well understood.

To investigate the interactions of vitamin D and PTH in mineral ion homeostasis and skeletal remodeling *in vivo*, we generated double knock-out mice which are homozygous for both the 1α(OH)ase null allele and the PTH null allele and compared these to the phenotypes of the corresponding single gene null mice and to wild-type mice.

RESULTS

Gene dosage effects

No apparent effects of gene dosage with respect to mineral or skeletal homeostasis were observed in heterozygotes or compound heterozygotes. Consequently, the phenotypes of $PTH^{+/-}1\alpha(OH)ase^{-/-}$ mice and $PTH^{-/-}1\alpha(OH)ase^{+/-}$ mice resembled those of $1\alpha(OH)ase^{-/-}$ mice and of $PTH^{-/-}$ mice, respectively, and the phenotype of $PTH^{+/-}1\alpha(OH)ase^{+/-}$ animals resembled that of the wild-type animals (data not shown). Therefore, subsequent results describe only those observed in homozygotes.

Alterations of biochemistry, size of parathyroid glands and expression of 1α(OH)ase and 24(OH)ase genes

At 2 weeks of age, both $PTH^{-/-}$ and $1\alpha(OH)ase^{-/-}$ mice displayed hypocalcemia, but the $PTH^{-/-}1\alpha(OH)ase^{-/-}$ mice displayed more severe hypocalcemia than either $PTH^{-/-}$ mice or $1\alpha(OH)ase^{-/-}$ mice (Fig. 1A). PTH deficiency caused hyperphosphatemia, whereas serum phosphorus levels were not significantly reduced in $1\alpha(OH)ase^{-/-}$ mice (Fig. 1B). Serum phosphorus was elevated in the double mutants reflecting the dominance of the PTH effects on renal clearance in determining serum phosphorus. Serum $1,25(OH)_2D_3$ levels were ample in $PTH^{-/-}$ mice, but were undetectable in $1\alpha(OH)ase^{-/-}$ mice and $PTH^{-/-}1\alpha(OH)ase^{-/-}$ mice (Fig. 1C). Serum PTH levels were undetectable in $PTH^{-/-}$ mice and $PTH^{-/-}1\alpha(OH)ase^{-/-}$ mice but were raised in $1\alpha(OH)ase^{-/-}$ mice (Fig. 1D).

The size of the parathyroid glands was significantly enlarged in the two PTH mutants and was only slightly enlarged in $1\alpha(OH)ase^{-/-}$ mice (Fig. 1E), despite the fact their serum PTH levels were raised significantly.

The 1α(OH)ase and 24(OH)ase mRNA expression levels in kidney were examined by real-time RT–PCR. Results revealed that the 1α(OH)ase mRNA was undetectable in $1\alpha(OH)ase^{-/-}$ mice and $PTH^{-/-}1\alpha(OH)ase^{-/-}$ mice. Levels were higher in the $PTH^{-/-}$ mice than in wild-type mice presumably due to up-regulation by low extracellular calcium despite PTH deficiency (Fig. 1F). Expression of the 24(OH)ase gene was not significantly altered in the $PTH^{-/-}$ mice, but was reduced dramatically in $1\alpha(OH)ase^{-/-}$ mice and less markedly in $PTH^{-/-}1\alpha(OH)ase^{-/-}$ mice (Fig. 1F). These alterations of 24(OH)ase gene levels *in vivo* are consistent with previous well established regulation patterns *in vitro*, i.e. $1,25(OH)_2D_3$ up-regulates, whereas PTH down-regulates the 24(OH)ase mRNA (17).

Alterations of expression levels of calcium transporters in kidney

Both PTH and $1,25(OH)_2D_3$ are known to alter calcium transport across renal epithelium. To determine whether there were alterations of expression levels of the transcellular calcium transport system, the expression of renal calcium transporters was examined by real-time RT–PCR and western blots. The results revealed that gene expression levels of TRPV5, calbindin-D_{28K}, calbindin-D_{9K} and the Na^+/Ca^{2+} exchanger (NCX1) in kidney were reduced in $PTH^{-/-}$ mice, more markedly reduced in $1\alpha(OH)ase^{-/-}$ mice and most dramatically reduced in $PTH^{-/-}1\alpha(OH)ase^{-/-}$ mice (Fig. 1G). Protein expression levels of TRPV5, calbindin-D_{28K}, calbindin-D_{9K} and NCX1 in the kidney were also reduced in $PTH^{-/-}$ mice and in $1\alpha(OH)ase^{-/-}$ mice and most dramatically in $PTH^{-/-}1\alpha(OH)ase^{-/-}$ mice

Downloaded from https://academic.oup.com/hmg/article/14/11/1515/605493 by guest on 20 April 2024

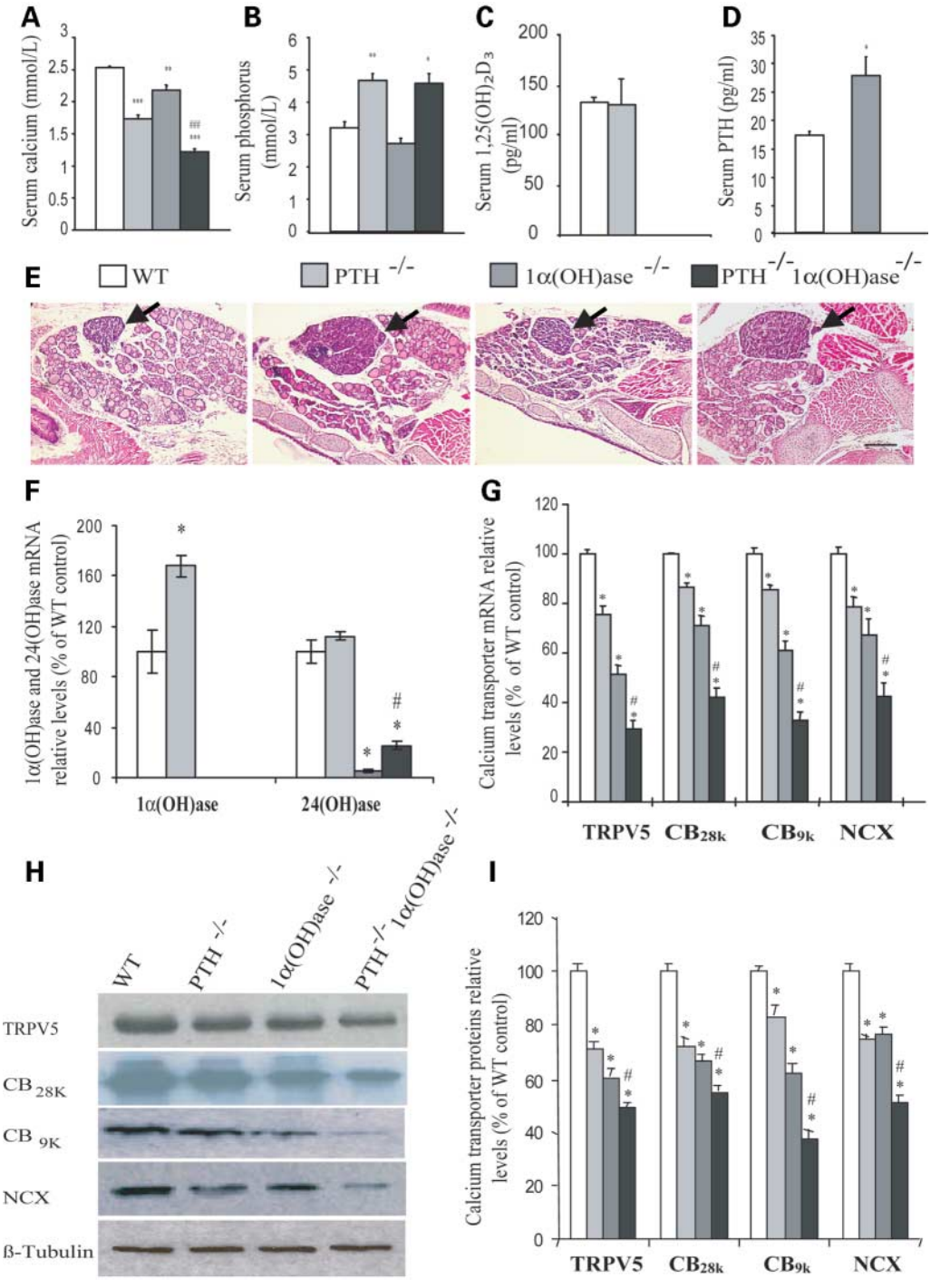

Figure 1. Serum chemistry, size of parathyroid glands, expression of 1α(OH)ase, 24(OH)ase genes and calcium transporters in kidney. Serum (**A**) calcium, (**B**) phosphorus, (**C**) $1,25(OH)_2D_3$ and (**D**) PTH were determined in sex-matched wild-type (WT), $PTH^{-/-}$, $1\alpha(OH)ase^{-/-}$ and $PTH^{-/-}$ $1\alpha(OH)ase^{-/-}$ mice as described in Materials and Methods. Each value is the mean ± SE of determinations in five mice of the same genotype. (**E**) Representative micrographs of parathyroid glands (arrows) and adjacent thyroid tissue of WT, $PTH^{-/-}$, $1\alpha(OH)ase^{-/-}$ and $PTH^{-/-}$ $1\alpha(OH)ase^{-/-}$ mice. Sections were stained with H&E, bar = 100 μm. (**F**) Comparison of 1α(OH)ase and 24(OH)ase gene expression levels in kidney of WT, $PTH^{-/-}$, $1\alpha(OH)ase^{-/-}$ and $PTH^{-/-}$ $1\alpha(OH)ase^{-/-}$ mice. Specific 1α(OH)ase and 24(OH)ase products were amplified from the tissue RNAs by real-time RT–PCR as described in Materials and Methods. Messenger RNA expression assessed by real-time RT–PCR analysis was calculated as a ratio to the GAPDH mRNA level and expressed relative to levels of WT mice. (**G**) Comparison of TRPV5, calbindin-D_{28K} (CB_{28K}), calbindin-D_{9K} (CB_{9K}) and Na^+/Ca^{2+} exchanger (NCX) expression in kidney of sex-matched wild-type (WT), $PTH^{-/-}$, $1\alpha(OH)ase^{-/-}$ and $PTH^{-/-}$ $1\alpha(OH)ase^{-/-}$ mice. Specific TRPV5, CB_{28K}, CB_{9K} and NCX products were amplified from the tissue RNAs by real-time RT–PCR as described in Materials and Methods. Messenger RNA expression assessed by real-time RT–PCR analysis was calculated as a ratio to the GAPDH mRNA level and expressed relative to levels of wild-type mice. (**H**) Western blots of long bone extracts for expression of TRPV5, CB_{28K}, CB_{9K} and NCX1. β-tubulin was used as loading control for western blots. (**I**) TRPV5, CB_{28K}, CB_{9K} and NCX protein levels relative to β-tubulin protein level were assessed by densitometric analysis and expressed relative to levels of wild-type mice. $^*P < 0.05$ compared with wild-type mice. $^{\#}P < 0.05$ compared with $PTH^{-/-}$ mice or $1\alpha(OH)ase^{-/-}$ mice.

Downloaded from https://academic.oup.com/hmg/article/14/11/1515/605493 by guest on 20 April 2024

(Fig. 1H and I). Although alterations of expression levels of calcium transporters were detected, no pathological changes were observed by H and E staining in the kidneys of any of the mutant animals (data not shown).

Skeletal alterations

To assess the action of $1,25(OH)_2D_3$ and potential interactions of $1,25(OH)_2D_3$ and PTH on skeletal development and bone remodeling, skeletal phenotypes of wild-type and the three mutant models were analyzed at 2 weeks of age. Overall body and long bone size, as shown by the skeletons of 2-week-old mice stained with alcian blue for cartilage and alizarin red for calcified skeletons, were reduced in all three mutant mice when compared with wild-type controls; however, the reductions were more severe in the $1\alpha(OH)ase^{-/-}$ and especially in the double mutants (Fig. 2A). Radiographs of femurs demonstrated that lengths of femurs were slightly reduced in $PTH^{-/-}$ mice, shorter in $1\alpha(OH)ase^{-/-}$ mice and shortest in $PTH^{-/-}1\alpha(OH)ase^{-/-}$ mice when compared with their wild-type littermates (Fig. 2B and F).

We examined the proximal end of tibiae and distal end of the femurs by micro-CT. Representative frontal views and longitudinal sections of three-dimensional reconstructed proximal ends of tibiae are shown in Figure 2C and D, respectively. Epiphyseal volumes were minimally reduced in hypocalcemic $PTH^{-/-}$ mice, markedly reduced in $1\alpha(OH)ase^{-/-}$ mice and most dramatically reduced in $PTH^{-/-}1\alpha(OH)ase^{-/-}$ mice (Fig. 2C and G). Unmineralized widened growth plate spaces were seen in $1\alpha(OH)ase^{-/-}$ mice which had $1,25(OH)_2D_3$ deficiency and mild hypocalcemia and especially in $PTH^{-/-}1\alpha(OH)ase^{-/-}$ mice which had $1,25\text{-}(OH)_2D_3$ deficiency and severe hypocalcemia (Fig. 2D). Both micro-CT and histology demonstrated that the trabecular bone volume was moderately diminished in $PTH^{-/-}$ mice and in $1\alpha(OH)ase^{-/-}$ mice, but markedly decreased in $PTH^{-/-}1\alpha(OH)ase^{-/-}$ mice (Fig. 2D, E and H).

Alterations of cartilaginous growth plates

We examined chondrocyte proliferation, differentiation and cartilage matrix mineralization to determine whether the shortening of long bones resulted from changes in endochondral bone formation. Owing to the delay of development of the secondary ossification center, residual hypertrophic chondrocytes were observed on the epiphyseal surface of the cartilaginous growth plates in the $1\alpha(OH)ase^{-/-}$ and in the $PTH^{-/-}1\alpha(OH)ase^{-/-}$ mice (Fig. 3A and D). These additional hypertrophic chondrocytes contributed to the unmineralized widened growth plate spaces seen by micro-CT in the $1\alpha(OH)ase^{-/-}$ and in the $PTH^{-/-}$ $\alpha(OH)ase^{-/-}$ mice (Fig. 2D). Proliferation of chondrocytes was not altered significantly in $PTH^{-/-}$ and $1\alpha(OH)ase^{-/-}$ mice, but was decreased significantly in $PTH^{-/-}1\alpha(OH)ase^{-/-}$ mice (Fig. 3B and G). The width of growth plates (Fig. 3A and E), hypertrophic zone (Fig. 3A and F) and the deposition of type X collagen in the matrix of the hypertrophic zone (Fig. 3C and H) were not significantly altered in $PTH^{-/-}$ mice and in $1\alpha(OH)ase^{-/-}$ mice, but were diminished in $PTH^{-/-}1\alpha(OH)ase^{-/-}$ mice. Mineralization of cartilage matrix was reduced in $PTH^{-/-}$ mice and $1\alpha(OH)ase^{-/-}$ mice and more dramatically in $PTH^{-/-}1\alpha(OH)ase^{-/-}$ mice (Fig. 3D and I).

Alterations of osteoblastic bone formation parameters

To determine whether the alterations of bone volume which were observed were associated with alterations of osteoblastic bone formation, we examined mineral apposition rate (MAR) and performed histomorphormetic analysis for osteoid volume, osteoblast number and type I collagen deposition in bone matrix. MAR was decreased in all three mutants and was reduced more significantly in $PTH^{-/-}1\alpha(OH)ase^{-/-}$ mice (Fig. 4A and C). Mineralization of trabecular and cortical bone was decreased in $PTH^{-/-}1\alpha(OH)ase^{-/-}$ mice when compared with wild-type mice, and osteoid volume was increased (Fig. 4B and D). Despite the decreased bone mineralization, fractures were not observed prior to their death in tetany within 3 weeks of birth. The osteoblast number (Fig. 5C), ALP and type I collagen positive areas (Fig. 5A, B, D and E) were reduced in both $PTH^{-/-}$ and $1\alpha(OH)ase^{-/-}$ mice when compared with wild-type mice and were reduced more significantly in $PTH^{-/-}1\alpha(OH)ase^{-/-}$ mice. We also examined the alterations in expression of genes related to bone formation. RNA was isolated from long bones and real time RT–PCR was performed. Results showed that gene expression of Cbfa I, ALP, type I collagen and osteocalcin were all reduced in $PTH^{-/-}$ and $1\alpha(OH)ase^{-/-}$ mice and even more dramatically reduced in the $PTH^{-/-}1\alpha(OH)ase^{-/-}$ mice (Fig. 5F). These alterations were consistent with the decreased osteoblastic bone formation observed by histomorphometric analysis. These results indicate that PTH and $1,25(OH)_2D_3$ each exert anabolic effects on the skeleton and also exert synergistic anabolic effects on bone.

Alterations of osteoclastic bone resorption parameters

We also investigated whether the decreased bone volume could be caused by increased osteoclastic bone resorption. TRAP positive osteoclast numbers were decreased significantly in both $PTH^{-/-}$ mice and $1\alpha(OH)ase^{-/-}$ mice when compared with wild-type mice. TRAP positive osteoclast number was also decreased in $PTH^{-/-}1\alpha(OH)ase^{-/-}$ mice when compared with wild-type mice, but not more than in either $PTH^{-/-}$ mice or $1\alpha(OH)ase^{-/-}$ mice (Fig. 6A and C). Receptor activator of NF-κB ligand (RANKL) immunoreactivity in osteoblastic cells was found to be low in all three mutants, but more dramatically in $PTH^{-/-}1\alpha(OH)ase^{-/-}$ mice, possibly reflecting lower levers of osteoblastic cells (Fig. 6B and D). The ratio of RANKL/OPG mRNA levels was decreased in bone of the mutants when compared with wild-type bone as demonstrated by real-time RT–PCR (Fig. 6E), but was not additively decreased in $PTH^{-/-}1\alpha(OH)ase^{-/-}$ mice when compared with single mutants. These results indicate that there are no synergistic effects of PTH and $1,25(OH)_2D_3$ to enhance bone resorption parameters.

Downloaded from https://academic.oup.com/hmg/article/14/11/1515/605493 by guest on 20 April 2024

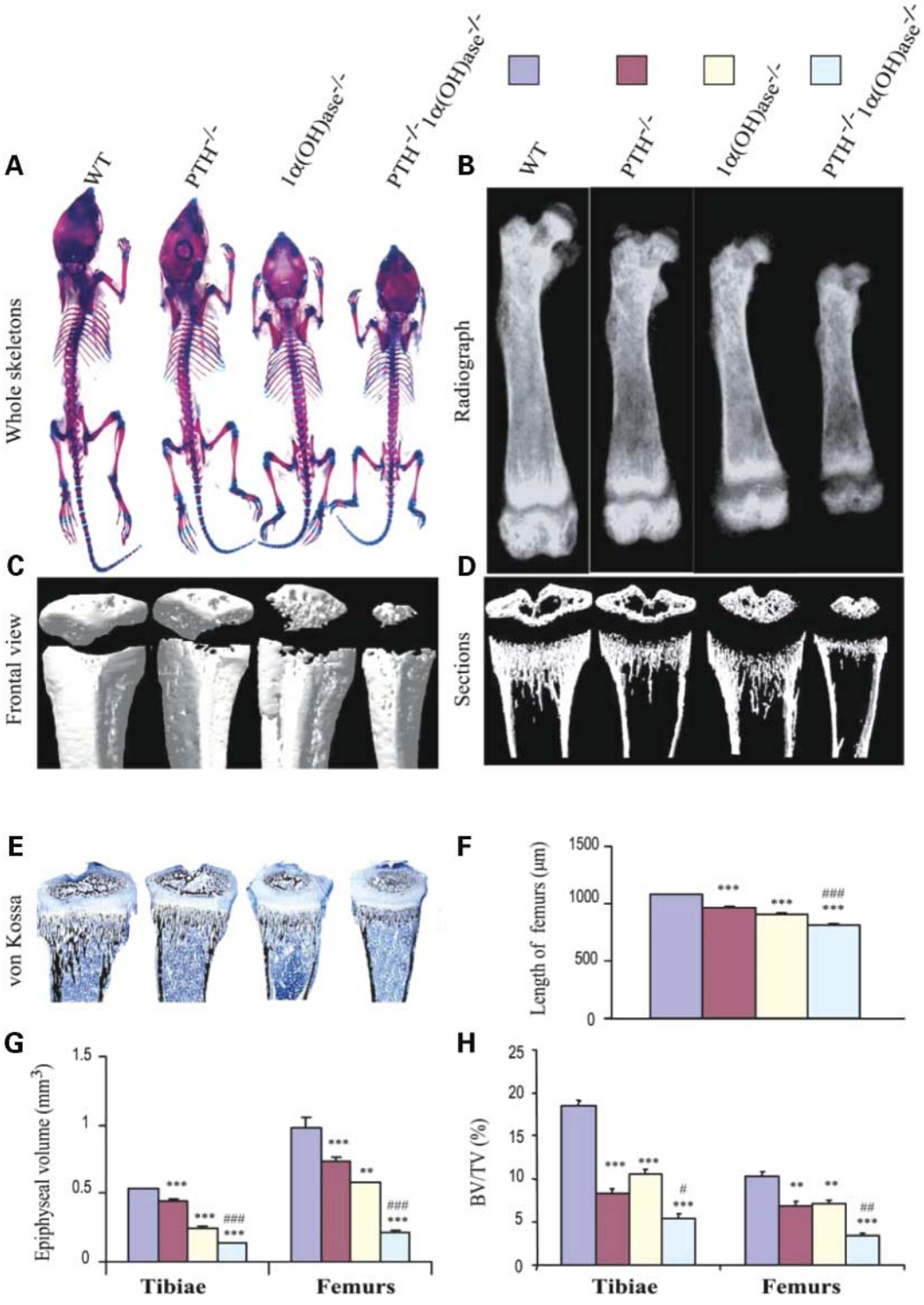

Figure 2. Skeletal phenotypes of mutant mice. (**A**) Whole mount skeletons at 2 weeks of age of the sex-matched wild-type (WT), $PTH^{-/-}$, $1\alpha(OH)ase^{-/-}$ and $PTH^{-/-}1\alpha(OH)ase^{-/-}$ mice were stained with Alcian blue (for cartilage) and alizarin red (for calcified tissue) as described in Materials and Methods. (**B**) Representative contact radiographs of the femurs of WT, $PTH^{-/-}$, $1\alpha(OH)ase^{-/-}$ and $PTH^{-/-}1\alpha(OH)ase^{-/-}$ mice. Representative (**C**) frontal views and (**D**) longitudinal sections of three-dimensional reconstructed proximal end of tibiae. (**E**) Representative micrographs from undecalcified sections of the proximal ends of tibiae stained by the von Kossa procedure as described in Materials and Methods and photographed at a magnification of 25×. (**F**) Quantitation of femoral length. (**G**) Quantitation of epiphyseal volume of the proximal ends of tibiae and the distal ends of femurs. (**H**) Trabecular bone volume was determined as described in Materials and Methods and is presented as percent of the tissue volume [BV/TV (%)] for each mutant. Each value is the mean ± SE of determinations in six sex-matched mice of the same genotype. $^{**}P < 0.01$; $^{***}P < 0.001$ compared with wild-type mice. $^{\#}P < 0.05$; $^{\#\#}P < 0.01$; $^{\#\#\#}P < 0.001$ compared with $PTH^{-/-}$ mice or $1\alpha(OH)ase^{-/-}$ mice.

Downloaded from https://academic.oup.com/hmg/article/14/11/1515/605493 by guest on 20 April 2024

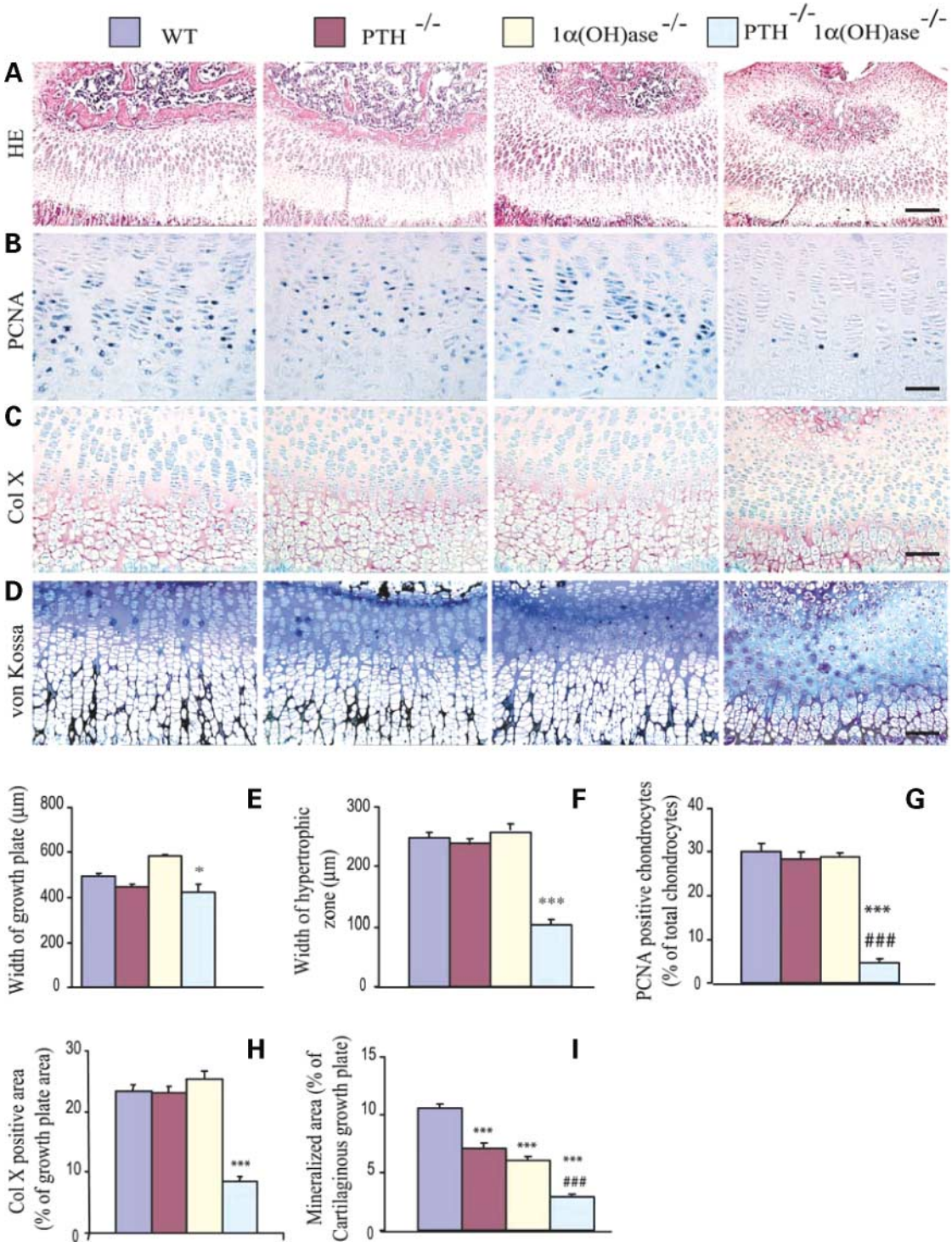

Figure 3. Assessment of indices of chondrocyte proliferation, differentiation and mineralization. Paraffin-embedded sections of tibiae from the sex-matched wild-type (WT), $PTH^{-/-}$, $1\alpha(OH)ase^{-/-}$ and $PTH^{-/-}1\alpha(OH)ase^{-/-}$ mice were (**A**) stained with H&E and immunostained for (**B**) PCNA or (**C**) type X collagen as described in Materials and Methods. Undecalcified sections of tibiae were stained by (**D**) the von Kossa procedure as described in Materials and Methods. Scale bars in A, B, C and D represent 100, 25, 50 and 50 μm, respectively. (**E**) Width of the cartilaginous growth plate and (**F**) width of hypertrophic zone in the mutants were determined as described in Materials and Methods. (**G**) Numbers of PCNA-positive chondrocytes of total chondrocytes per field were determined by image analysis, and the PCNA-positive percentages of total chondrocytes are presented as the mean ± SE of triplicate determinations. (**H**) Type X collagen immunopositive area as a percentage of the growth plate field was determined. The percent-positive area is presented as mean ± SE of triplicate determinations. (**I**) Mineralized area as a percent of the cartilage matrix per field was determined by image analysis and is presented as the mean ± SE of triplicate determinations. $^{*}P < 0.05$; $^{**}P < 0.01$; $^{***}P < 0.001$ in the sex-matched mutant mice relative to the wild-type mice. $^{\#\#\#}P < 0.001$ compared with $PTH^{-/-}$ mice or $1\alpha(OH)ase^{-/-}$ mice.

Downloaded from https://academic.oup.com/hmg/article/14/11/1515/605493 by guest on 20 April 2024

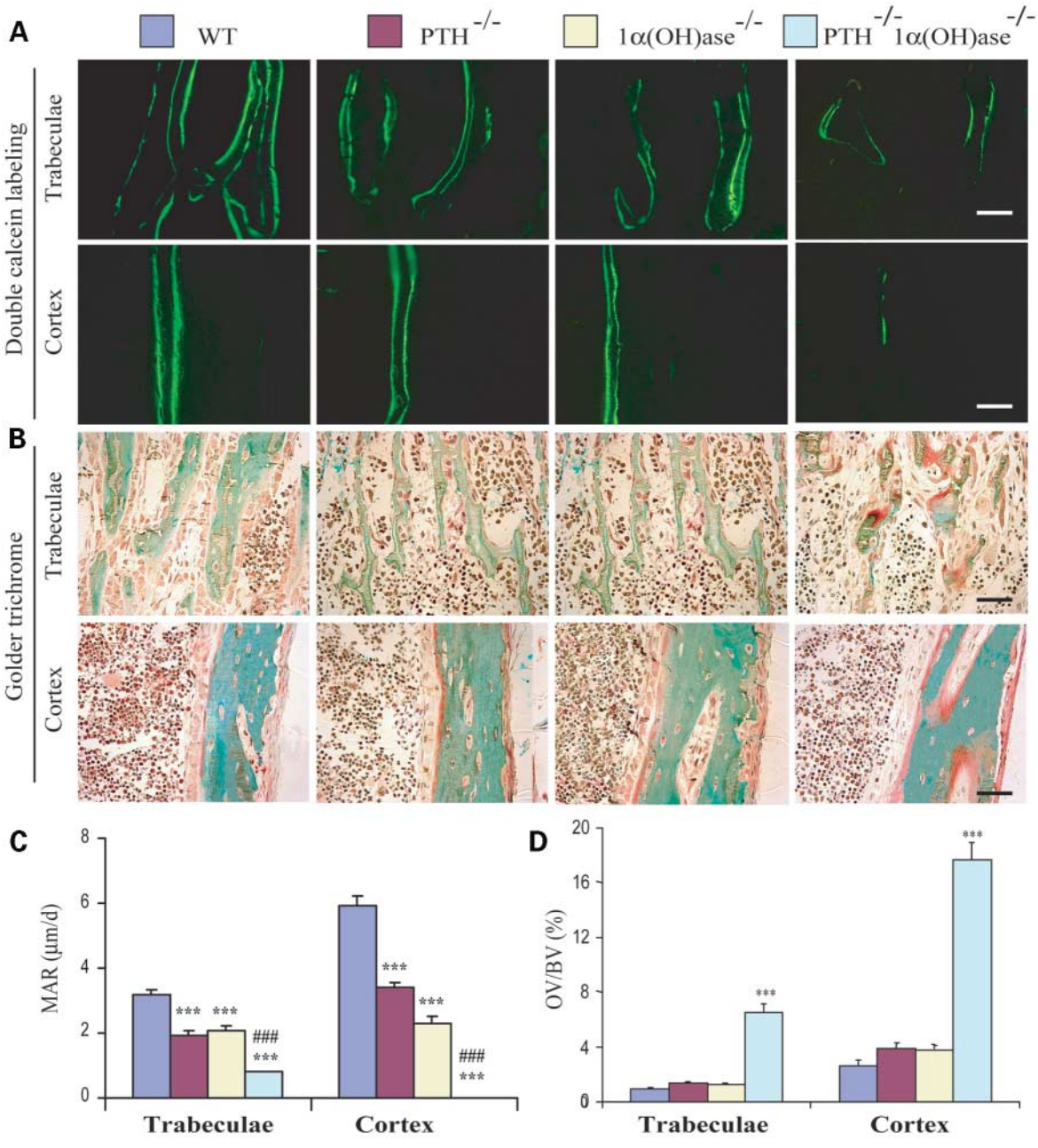

Figure 4. MAR and osteoid volume. Representative micrographs of (**A**) calcein double labeling and (**B**) sections stained by Goldner trichrome method in the trabeculae and cortex were imaged from ethanol fixed and undecalcified LR White resin embedded sections of the proximal ends of tibiae of the sex-matched wild-type (WT), $PTH^{-/-}$, $1\alpha(OH)ase^{-/-}$ and $PTH^{-/-}1\alpha(OH)ase^{-/-}$ mice. Scale bars in A and B represent 25 and 40 μm, respectively. (**C**) MAR of trabeculae and cortex of the same animals was determined as described in Materials and Methods. (**D**) Osteoid volume was determined in undecalcified sections stained with Goldner trichrome method and is presented as a percent of bone volume [OV/BV (%)] of trabeculae and of cortex. Each value is the mean ± SE of determinations in six animals of the same genotype. $^{***}P < 0.001$ relative to sex-matched wild-type mice. $^{\#\#\#}P < 0.001$ compared with $PTH^{-/-}$ mice or $1\alpha(OH)ase^{-/-}$ mice.

DISCUSSION

In the present study, we generated a novel genetically altered mouse model, which is homozygous for both the PTH null allele and the 1α(OH)ase null allele and compared this with null mice in which each individual gene is ablated and which depict phenotypes corresponding to loss-of-function mutations in the human PTH and 1α(OH)ase genes. Although both the $PTH^{-/-}$ and the $1\alpha(OH)ase^{-/-}$ mice developed hypocalcemia with moderate skeletal defects, they were viable. The $1\alpha(OH)ase^{-/-}PTH^{-/-}$ mice died within 3 weeks postnatally, prior to the end of weaning, with severe hypocalcemia and tetany. Serum $1,25(OH)_2D_3$ concentrations were not suppressed in the $PTH^{-/-}$ mice, reflecting the

Downloaded from https://academic.oup.com/hmg/article/14/11/1515/605493 by guest on 20 April 2024

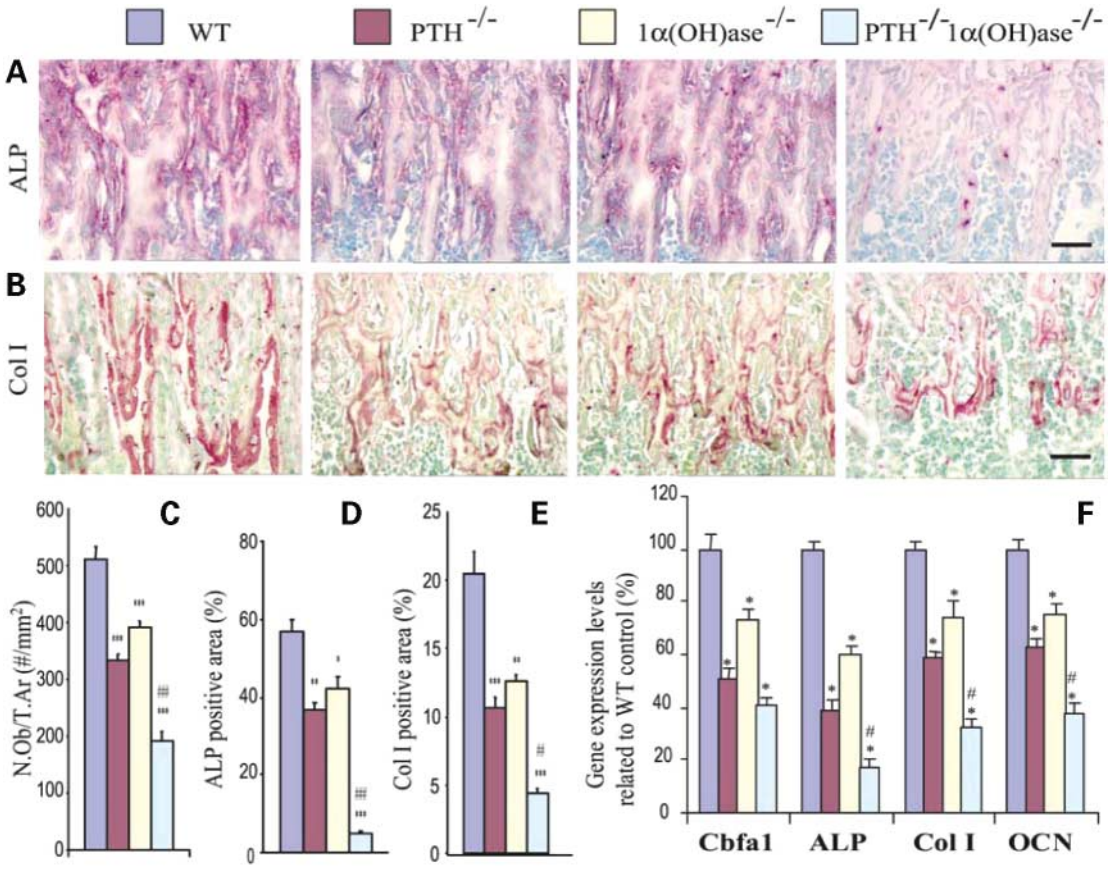

Figure 5. Assessment of bone formation parameters. Representative micrographs of tibial sections from the sex-matched wild-type (WT), $PTH^{-/-}$, $1\alpha(OH)ase^{-/-}$ and $PTH^{-/-}1\alpha(OH)ase^{-/-}$ mice, stained histochemically for (**A**) ALP and (**B**) immunostained for type I collagen (Col I). The bar = 25 μm. (**C**) Number of osteoblasts per mm^2 was counted in the primary spongiosa of H&E-stained tibiae and presented as mean ± SE. The (**D**) ALP and (**E**) type I collagen positive area as a percent of the tissue area were determined in the metaphyseal regions for each mutant. (**F**) Real-time RT–PCR of long bone extracts for the expression of Cbfa I, ALP, Col I and osteocalcin (OCN). Messenger RNA expression assessed by real-time RT–PCR is calculated as a ratio to the GAPDH mRNA level and expressed relative to levels of wild-type mice. Each value is the mean ± SE of determinations in six animals of the same genotype. $^{*}P < 0.05$; $^{**}P < 0.01$; $^{***}P < 0.001$ in the sex-matched mutant mice relative to the wild-type mice. $^{\#}P < 0.05$; $^{\#\#}P < 0.01$; $^{\#\#\#}P < 0.001$ compared with $PTH^{-/-}$ mice or $1\alpha(OH)ase^{-/-}$ mice.

predominant role of hypocalcemia, relative to PTH, in modulating 1α(OH)ase activity at this stage of development. In our previous studies in 4-month-old $PTH^{-/-}$ mice, $1,25(OH)_2D_3$ concentrations were indeed noted to be low, but even in these animals, 1α(OH)ase activity and $1,25(OH)_2D_3$ concentrations could be stimulated by a low calcium intake (12).

In view of the fact that both PTH and $1,25(OH)_2D_3$ modulate active renal transcellular transport which is a pivotal process in the regulation of calcium homeostasis, we examined the changes in transcellular calcium transporters in the three mutant mouse models and compared them with their wild-type littermates. Active transcellular transport is a multi-step process. It includes a rate-limiting step of entry of calcium from the renal tubular lumen through the apical tetrameric epithelial channel, TRPV5, diffusion of calbindin-bound calcium to the basolateral membrane and extrusion of calcium into the blood via a sodium–calcium exchanger (NCX1). Our results showed that mRNA and protein levels of TRPV5, calbindin-D_{9K}, calbindin-D_{28K} and NCX1 in kidney were reduced independently in the $1,25(OH)_2D_3$ replete $PTH^{-/-}$ mice and in the PTH replete $1\alpha(OH)ase^{-/-}$ mice. This is in line with a diminished capacity for renal calcium re-absorption contributing to the development of hypocalcemia in the $PTH^{-/-}$ mice and $1\alpha(OH)ase^{-/-}$ mice. Our results in $1\alpha(OH)ase^{-/-}$ mice are consistent with a previous report (18), which demonstrated that the expression of the renal Ca^{2+} transport proteins TRPV5, calbindin-D_{28K}, calbindin-D_{9K} and NCX1 was significantly down-regulated in the kidney using a different 1α(OH)ase deficient animal model (14). Our results in $PTH^{-/-}$ mice demonstrating decreased renal calcium transport protein expression are consistent with previous preliminary results in parathyroidectomized rats (19) and with previous results demonstrating direct regulation of TRPV5 by PTH *in vitro* (20). Taken together, these results suggest that PTH and $1,25(OH)_2D_3$ can each independently, but also cooperatively, regulate transcellular calcium transport in the kidney.

Our current observations show that at 2 weeks of age, $PTH^{-/-}$ mice had few abnormalities of the cartilaginous growth plate other than reduced mineralization at the chondro-osseous junction with an associated slight reduction in long bone length. This is analogous to the phenotype of

Downloaded from https://academic.oup.com/hmg/article/14/11/1515/605493 by guest on 20 April 2024

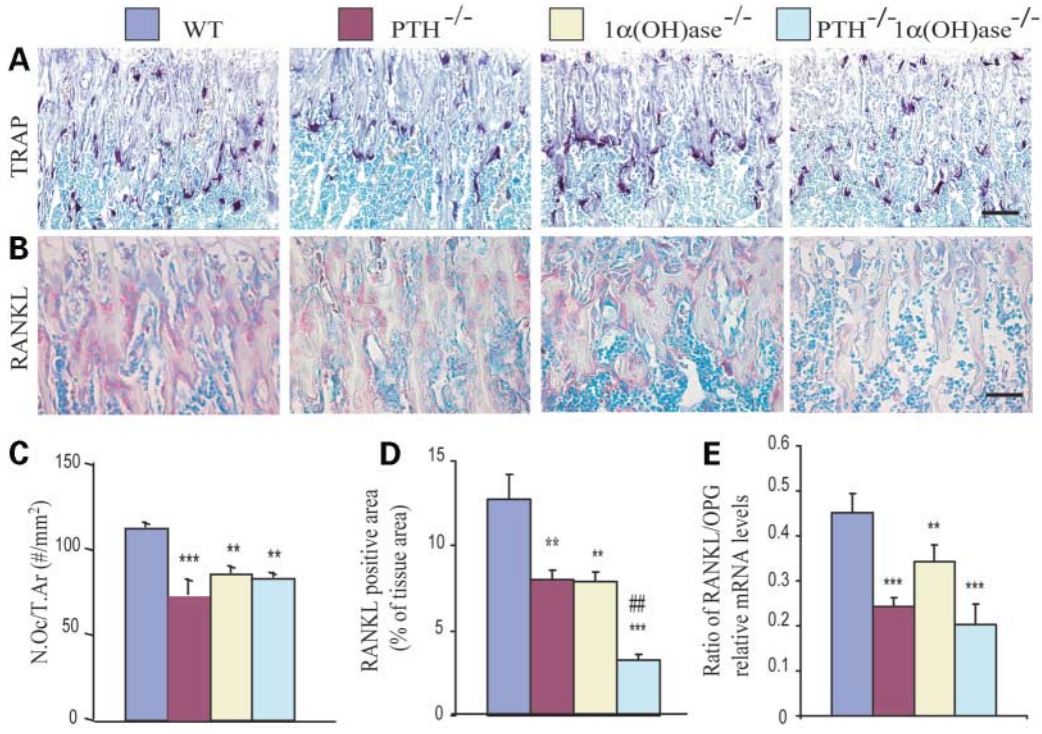

Figure 6. Assessment of bone resorption parameters. Representative micrographs of sections of the tibial metaphysis (**A**) stained histochemically for TRAP and (**B**) immunostained for RANKL in the sex-matched wild-type (WT), $PTH^{-/-}$, $1\alpha(OH)ase^{-/-}$ and $PTH^{-/-}1\alpha(OH)ase^{-/-}$ mice. Scale bars in A and B represent 50 and 25 μm, respectively. (**C**) Number of TRAP positive osteoclasts per mm^2 of tissue and (**D**) RANKL immunopositive area relative to tissue area. Each value is the mean ± SE of determinations in six animals of the same genotype. (**E**) Real-time RT–PCR was performed on bone extracts for RANKL and OPG mRNA as described in Materials and Methods. Messenger RNA expression assessed by real-time RT–PCR analysis is calculated as a ratio to the GAPDH mRNA level and expressed relative to levels of wild-type mice. Ratio of RANKL/OPG relative mRNA levels was calculated and was presented as the mean ± SE of determinations in six animals of the same genotype. $^{**}P < 0.01$ and $^{***}P < 0.001$ relative to wild-type mice. $^{\#\#}P < 0.01$compared with $PTH^{-/-}$ mice or $1\alpha(OH)ase^{-/-}$ mice.

newborn $PTH^{-/-}$ mice, which we have previously reported (21). We (13) and others (14) have also previously reported the skeletal phenotypes of $1\alpha(OH)ase^{-/-}$ mice. Several months after weaning, $1\alpha(OH)ase^{-/-}$ mice maintained on a normal calcium intake develop skeletal abnormalities characteristic of severe rickets. However, no skeletal abnormality was detected in $1\alpha(OH)ase^{-/-}$ newborn mice (data not shown). This observation suggests that the skeletal action of $1,25(OH)_2D_3$ may be unnecessary *in utero* and that calcium alone is required and is in adequate supply due to the maternal contribution to the fetus. In contrast, clear abnormalities of the epiphyses, including the growth plate, were observed in 2-week-old $1\alpha(OH)ase^{-/-}$ mice prior to weaning. These included diminished development of the center of secondary ossification which most probably involved reduced vascular invasion, a process which we have previously reported, in studies *in vitro*, can be regulated by $1,25(OH)_2D_3$ (22). Failure to remodel the cartilaginous growth plate in the poorly developed secondary ossification site may therefore have contributed to the persistence of hypertrophic chondrocytes on this region which accounted for the overall widening of the growth plate in $1\alpha(OH)ase^{-/-}$ mice. In addition, reduced mineralization was seen. Such findings were not previously reported in $VDR^{-/-}$ mice (23,24) where only minor expansion of the zone of hypertrophic chondrocytes was detected at day 15 (25). It remains to be determined whether these differences between the alterations in the ligand deficiency model and the receptor deficiency model reflect a genomic or a non-genomic action of $1,25(OH)_2D_3$, perhaps mediated by increases in PKC activity as has been reported in mouse chondrocytes *in vitro* (26). Despite the alterations seen in this region of bone at 2 weeks of age, $1\alpha(OH)ase^{-/-}$ mice fed a normal or high calcium intake exhibited an even more severe alteration when analyzed at 4 months, with marked distortion of the growth plate. At 4 months, $1\alpha(OH)ase^{-/-}$ mice manifest more severe hyperparathyroidism (27) and more severe hypophosphatemia. It is likely therefore that, as in hypophosphatemic (Hyp) mice (28,29), the more severe hypophosphatemia in the older $1\alpha(OH)ase^{-/-}$ mice contributes to the pronounced disorganization and more severe demineralization of the cartilaginous growth plate.

However, at 2 weeks of age, the most severe alteration in the epiphyseal region of bone was observed in the double mutants rather than the single mutants and included a reduction of proliferating chondrocytes. Such abnormalities may have been due to the more severe hypocalcemia prevailing in the double mutants in view of the fact that calcium *per se* has been reported to modulate the chondrocyte life cycle (30).

Downloaded from https://academic.oup.com/hmg/article/14/11/1515/605493 by guest on 20 April 2024

We previously reported that newborn $PTH^{-/-}$ mice had decreased osteoblast numbers and diminished trabecular bone volume demonstrating that PTH is essential for fetal trabecular bone formation (21). Our current observation shows that the phenotype of the $PTH^{-/-}$ mice at 2 weeks of age was similar to that of newborn mice in that trabecular bone volume, MAR, osteoblast numbers, ALP activity in osteoblasts and type I collagen deposition in bone matrix were all reduced when compared with wild-type littermates. We also demonstrated that gene expression levels of Cbfa1, ALP, type I collagen and osteocalcin were reduced in $PTH^{-/-}$ mice consistent with the decreased osteoblastic bone formation observed by morphological analysis.

Diminished trabecular bone volume, reduced osteoblastic bone formation parameters and decreased gene expression levels of indices of the osteoblastic phenotype were also observed in 2-week-old PTH-replete $1\alpha(OH)ase^{-/-}$ mice, indicating that PTH and $1,25(OH)_2D_3$ exert independent effects on osteoblastic bone formation. We previously reported that trabecular bone volume was reduced in 4-month-old $1\alpha(OH)ase^{-/-}$ mice when fed a 'rescue diet' which normalized serum calcium and PTH levels (27). The present studies in 2-week-old mice confirmed those observations even in the face of a modest increase in serum PTH levels and mild hypocalcemia of relatively short duration. Our results therefore point to a physiological anabolic role of endogenous $1,25(OH)_2D_3$ *in vivo* and are consistent with reports of a pharmacological anabolic role for exogenous $1,25(OH)_2D_3$ when administered *in vivo* (31).

Overall, PTH deficiency caused only a slight reduction in long bone length, but resulted in a marked reduction in trabecular bone volume and osteoblast numbers in the metaphyseal region. In contrast, $1,25(OH)_2D_3$ deficiency caused a somewhat smaller reduction in trabecular bone volume and osteoblast numbers in the metaphyseal region, but a marked reduction in long bone length and epiphyseal volume. These differences suggest that PTH exerts its anabolic effects on bone predominantly by stimulating appositional osteoblastic bone formation, whereas $1,25(OH)_2D_3$ exerts its anabolic effect predominantly through stimulating endochondral bone formation. The most severe skeletal development defects were observed in the double mutants where in the absence of both PTH and $1,25(OH)_2D_3$, severe impairment in both appositional and endochondral bone formation was observed, leading to the shortest long bones and the most profound impairment of trabecular bone volume. These results indicate that synergistic actions of PTH and $1,25(OH)_2D_3$ are needed to stimulate bone appositional and endochondral bone formation.

Although PTH and $1,25(OH)_2D_3$ can each exert a skeletal catabolic action, we have not observed any synergistic effect on osteoclastic bone resorption in the double mutants. Our results show that TRAP positive osteoclast numbers were decreased significantly in both $PTH^{-/-}$ mice and $1\alpha(OH)ase^{-/-}$ mice when compared with wild-type mice, but were not further decreased in double mutants compared with either $PTH^{-/-}$ mice or $1\alpha(OH)ase^{-/-}$ mice. Although other factors are also involved in regulating osteoclastic bone resorption, these factors therefore cannot apparently replace the function of $1,25(OH)_2D_3$ and PTH in their action to resorb bone.

Table 1. Summary of the effects of PTH and 1α(OH)ase deficiency on mineral and skeletal homeostasis

	$PTH^{-/-}$	$1\alpha(OH)ase^{-/-}$	$PTH^{-/-}$ $1\alpha(OH)ase^{-/-}$
Mineral ion homeostasis			
Ca	↓	↓	↓ ↓
P	↑	↓	↑
Renal Ca transporters	↓	↓ ↓	↓ ↓ ↓
Epiphyseal changes			
Size of epiphysis	↓ →	↓	↓ ↓
Chondrocyte proliferation	→	→	↓
Chondrocyte differentiation	→	→	↓
Growth plate mineralization	↓	↓	↓ ↓
Long bone length	↓ →	↓	↓ ↓
Bone changes			
Osteoblast production	↓ ↓	↓	↓ ↓ ↓
Osteoclast production	↓	↓	↓
Trabecular bone volume	↓ ↓	↓	↓ ↓ ↓
Bone mineralization	→	↓ →	↓

↓, a reduction; ↑, an increase; ↓ →, minimal change or a slight decrease and →, no change. Repetitive arrows indicate the magnitude of the change.

PTH and $1,25(OH)_2D_3$-mediated fluxes of calcium across intestine, bone and kidney are known to maintain extracellular calcium homeostasis. Although $1,25(OH)_2D_3$ is the major hormonal mediator enhancing active calcium absorption in the intestine, the complete absence of $1,25(OH)_2D_3$ by itself did not produce sufficient hypocalcemia to impair viability either in our present studies in mice with targeted ablation of the 1α(OH)ase gene or in previous studies in older animals. Consequently, $1,25(OH)_2D_3$-dependent reduction in intestinal calcium absorption did not appear to be the determining factor in producing lethal hypocalcemia in our double mutants. When $1,25(OH)_2D_3$-deficient mice were made PTH-deficient i.e. in the double mutants, no change in the already diminished bone resorption was observed, indicating that altered bone resorption could not account for the further decrease in serum calcium as seen in the double mutants. In contrast, the absence of both PTH and $1,25(OH)_2D_3$ markedly further reduced the mediators of active calcium transport, suggesting that impaired renal conservation was a major determinant of the lethal hypocalcemia in the double mutants.

Overall, our studies also show that PTH and $1,25(OH)_2D_3$ acting in the neonatal period, independently or co-operatively in bone and kidney (Table 1), have effects for which apparently no redundancy has evolved to conserve calcium homeostasis for postnatal animal survival.

MATERIALS AND METHODS

Derivation of PTH and 1α(OH)ase double null mice

The derivation of the two parental strains of $PTH^{-/-}$ mice and $1\alpha(OH)ase^{-/-}$ mice by homologous recombination in embryonic stem cells was previously described by Miao *et al.* (12,21) and Panda *et al.* (13), respectively. Briefly, a neomycin resistance gene was inserted into exon III of the

Downloaded from https://academic.oup.com/hmg/article/14/11/1515/605493 by guest on 20 April 2024

mouse *Pth* gene replacing the entire mature PTH coding sequence. Lack of PTH expression was confirmed by immunostaining of parathyroid gland sections (21). A neomycin resistance gene replaced exons VI, VII and VIII of the mouse 1α(OH)ase gene removing both the ligand binding and the heme binding domains (13). RT–PCR of renal RNA from homozygous $1\alpha(OH)ase^{-/-}$ mice confirmed the lack of 1α(OH)ase expression. $PTH^{+/-}$ mice and $1\alpha(OH)ase^{+/-}$ mice were fertile and were mated to produce offspring heterozygous at both loci, which were then mated to generate $PTH^{-/-}$ $1\alpha(OH)ase^{-/-}$ pups. Lines were maintained by mating $PTH^{+/-}$ $1\alpha(OH)ase^{+/-}$ males and $PTH^{+/-}$ $1\alpha(OH)ase^{+/-}$ females on a mixed genetic background with contributions from C57BL/6J and BALB/c strains.

Genotyping of mice

Tail fragment genomic DNA was isolated by standard phenol–chloroform extraction and isopropanol precipitation. To genotype at the PTH and 1α(OH)ase loci, four PCRs were conducted. The presence of the wild-type *Pth* allele was detected using PTH forward primer, 5′-GATGTCTG CAAACACCGTGGCTAA-3′ and PTH reverse primer, 5′-TCCAAAGTTTCATTACAGTAGAAG-3′. The null *Pth* allele was detected using Neo forward primer 5′-TCTTGATTCCCACTTTGTGGTTCTA-3′ and PTH reverse primer (32). For the wild-type 1α(OH)ase allele, forward primer, 5′-AGACTGCACTCCACTCTGAG-3′ and reverse primer, 5′-GTTTCCTACACGGATGTCTC-3′ were used. The neomycin gene was detected with primers neo-F, 5′-ACAACAGACAATCGGCTGCTC-3′, and neo-R, 5′-CCATGGGTCACGACGAGATC-3′ (27).

Quantitative real-time PCR

Reverse transcription reactions were performed using the SuperScript First-Strand Synthesis System (Invitrogen) as previously described (33). Real-time PCR was performed using a LightCycler system (Roche Molecular Biochemicals, Indianapolis, IN, USA). The conditions were 2 μl of LightCycler DNA master SYBR Green I (Roche), 0.25 μM of each 5′ and 3′ primer (Table 2) and 2 μl of sample and/or H_2O to a final volume of 20 μl. The $MgCl_2$ concentration was adjusted to 3 mM. Samples were amplified for 35 cycles with a temperature transition rate of 20°C/s for all three steps which were denaturation at 95°C for 10 s, annealing for 5 s and extension at 72°C for 20 s. SYBR Green fluorescence was measured to determine the amount of double-stranded DNA. To discriminate specific from non-specific cDNA products, a melting curve was obtained at the end of each run. Products were denatured at 95°C for 3 s, the temperature was then decreased to 58°C for 15 s and raised slowly from 58 to 95°C using a temperature transition rate of 0.1°C/s. To determine the number of copies of target DNA in the samples, purified PCR fragments of known concentration were serially diluted and served as external standards for each experiment. Data were normalized to GAPDH levels.

Table 2. Real-time RT–PCR primers used with their name, orientation (S, sense; AS, anti-sense), sequence, annealing temperature (T_m) and length of amplicon (bp)

Name	S/AS	Sequence	T_m (°C)	bp
1α(OH)ase	S	GCAGAGGCTCCGAAGTCTTC	58	729
	AS	TGTCTGGGACACGGGAATTC		
24(OH)ase	S	ACCGTGGACAGAACGCAATGG	58	500
	AS	AAATCCAGAGCGTGCTGCCTG		
TRPV5	S	CGTTGGTTCTTACGGGTTGAAC	55	141
	AS	GTTTGGAGAACCACAGAGCCTCTA		
calbindin-D_{28K}	S	GCAGAATCCCACCTGCAGTCATCTCTG	58	534
	AS	AAGAAGGAAATTTTCCTGCACTGGTAG		
calbindin-D_{9K}	S	CACTGACTGGTTGAGCAGGC	58	289
	AS	GAACTCCTTCTTCCTGACTTG		
NCX1	S	TCCCTACAAAACTATTGAAGGCACA	55	141
	AS	TTTCTCATACTCCTCGTCATCGATT		
Cbfa I	S	GTGACACCGTGTCAGCAAAG	55	356
	AS	GGAGCACAGGAAGTTGGGAC		
ALP	S	CTTGCTGGTGGAAGGAGGCAGG	55	393
	AS	CACGTCTTCTCCACCGTGGGTC		
α (I)	S	TCTCCACTCTTCTAGTTCCT	55	269
Procollagen	AS	TTGGGTCATTTCCACATGC		
Osteocalcin	S	CAAGTCCCACACAGCAGCTT	55	370
	AS	AAAGCCGAGCTGCCAGAGTT		
RANKL	S	GGTCGGGCAATTCTGAATT	55	813
	AS	GGGGAATTACAAAGTGCACCAG		
OPG	S	TGGAGATCGAATTCTGCTTG	55	719
	AS	TCAAGTGCTTGAGGGCATAC		
GAPDH	S	GGTCGGTGTGAACGGATTTG	55	508
	AS	ATGAGCCCTTCCACAATG		

Biochemical and hormone analyses

Serum calcium and phosphorus were determined by autoanalyzer (Beckman Synchron 67; Beckman Instruments). Serum $1,25(OH)_2D_3$ was measured by radioimmunoassay (Immuno-Diagnostic Systems, Bolden, UK) and intact PTH was measured by a two-site immunoradiometric assay (Immutopics, San Clemente, CA, USA).

Western blot analysis

Proteins were extracted from kidneys and quantitated by a kit (Bio-Rad, Mississauga, Ontario, Canada). In total, 30 μg protein samples were fractionated by SDS–PAGE and transferred to nitrocellulose membranes. Immunoblotting was carried out as described (34) using TRPV5 (ECaC1), calbindin-D_{28K}, calbindin-D_{9K} and NCX1 (Swant, Switzerland) and β-tubulin (Santa Cruz Biotechnology Inc., Santa Cruz, CA, USA). Bands were visualized using ECL chemiluminescence (Amersham) and quantitated by Scion Image Beta 4.02 (Scion Corporation, NIH).

Skeletal radiography

Femurs were removed and dissected free of soft tissue. Contact radiographs were taken using a Faxitron model 805 radiographic inspection system (Faxitron Contact, Faxitron, Germany) (22 kV voltage and 4 min exposure time). X-Omat TL film (Eastman Kodak Co., Rochester, NY, USA) was used and processed routinely.

Downloaded from https://academic.oup.com/hmg/article/14/11/1515/605493 by guest on 20 April 2024

Micro-computed tomography

Tibiae and femurs obtained from 2-week-old mice were dissected free of soft tissue, fixed overnight in 70% ethanol and analyzed by micro-CT with a SkyScan 1072 scanner and associated analysis software (SkyScan, Antwerp, Belgium) as described (33). Briefly, image acquisition was performed at 100 kV and 98 μA with a 0.9° rotation between frames. During scanning, the samples were enclosed in tightly fitting plastic wrap to prevent movement and dehydration. Thresholding was applied to the images to segment the bone from the background. Two-dimensional images were used to generate three-dimensional renderings using the 3D Creator software supplied with the instrument. The resolution of the micro-CT images is 18.2 μm.

Histology

Thyroparathyroid tissue, kidneys and tibiae were removed and fixed in PLP fixative (2% paraformaldehyde containing 0.075 M lysine and 0.01 M sodium periodate) overnight at 4°C and processed histologically as described (28). Proximal ends of tibiae were decalcified in ethylene-diamine tetra-acetic acid (EDTA) glycerol solution for 5–7 days at 4°C. Decalcified tibiae and other tissues were dehydrated and embedded in paraffin after which 5 μm sections were cut on a rotary microtome. The sections were stained with hematoxylin and eosin (H&E) or histochemically for alkaline phosphatase activity (ALP) or tartrate resistant acid phosphatase (TRAP) activity or immunohistochemical staining as described subsequently. Alternatively, undecalcified tibiae were embedded in LR White acrylic resin (London Resin Company Ltd, London, UK) and 1 μm sections were cut on an ultramicrotome. These sections were stained for mineral with the von Kossa staining procedure and counterstained with toluidine blue or by Goldner trichrome method.

Immunohistochemical staining

Proliferating cell nuclear antigen (PCNA), type I and X collagens and RANKL were determined by immunohistochemistry as described (21,28,29,33). Mouse monoclonal antibody against proliferating cell nuclear antigen (PCNA, Medicorp, Montreal, Canada), affinity-purified goat anti-human type I collagen antibody (Southern Biotechnology Associates, Birmingham, AL, USA), rabbit anti-serum to type X collagen (a generous gift of Dr A.R. Poole, Shriners Hospital, Montreal, Canada) and affinity purified goat polyclonal antibody raised against a peptide mapping at the C-terminal of RANKL (C-20, Santa Cruz Biotechnology Inc.) were applied to de-waxed paraffin sections overnight at room temperature. As a negative control, the pre-immune serum was substituted for the primary antibody. After washing with high salt buffer (50 mM Tris–HCl, 2.5% NaCl, 0.05% Tween 20, pH 7.6) for 10 min at room temperature followed by two 10 min washes with TBS, the sections were incubated with secondary antibody (biotinylated goat anti-rabbit IgG or biotinylated rabbit anti-goat IgG, Sigma), washed as before and incubated with the Vectastain ABC-AP kit or the Vectastain Elite ABC kit (Vector Laboratories, Inc. Ontario, Canada) for 45 min. After washing as before, red pigmentation to demarcate regions of immunostaining was produced by a 10–15 min treatment with fast red TR/naphthol AS-MX phosphate (Sigma; containing 1 mM levamisole as endogenous ALP inhibitor) or gray pigmentation was likewise produced using a Vector SG kit (Vector Laboratories, Inc.). After washing with distilled water, the sections were counterstained with methyl green and mounted with Kaiser's glycerol jelly.

Histochemical staining for collagen, ALP and TRAP

Enzyme histochemistry for ALP activity was performed as described (35,36). Briefly, following preincubation overnight in 1% magnesium chloride in 100 mm Tris–maleate buffer (pH 9.2), de-waxed sections were incubated for 2 h at room temperature in a 100 mM Tris–maleate buffer containing naphthol AS-MX phosphate (0.2 mg/ml, Sigma) dissolved in ethylene glycol monomethyl ether (Sigma) as substrate and fast red TR (0.4 mg/ml, Sigma) as a stain for the reaction product. After washing with distilled water, the sections were counterstained with Vector methyl green nuclear counterstain (Vector laboratories) and mounted with Kaiser's glycerol jelly.

Enzyme histochemistry for TRAP was performed as described (37). De-waxed sections were pre-incubated for 20 min in buffer containing 50 mM sodium acetate and 40 mM sodium tartrate at pH 5.0. Sections were then incubated for 15 min at room temperature in the same buffer containing 2.5 mg/ml naphthol AS-MX phosphate (Sigma) in dimethyl-formamide as substrate, and 0.5 mg/ml fast garnet GBC (Sigma) as a color indicator for the reaction product. After washing with distilled water, the sections were counterstained with methyl green and mounted in Kaiser's glycerol jelly.

Double calcein labeling

Double calcein labeling was performed by intra-peritoneal injection of mice with 10 μg calcein/g body weight (C-0875, Sigma) at 8 days and 3 days prior to sacrifice as described (12). Bones were harvested and embedded in LR White acrylic resin as described earlier. Serial sections were cut and the freshly cut surface of each section was viewed and imaged using fluorescence microscopy. The double calcein labeled width of cortex and trabeculae was measured using Northern Eclipse image analysis software v6.0 (Empix Imaging Inc., Mississauga, Ontario, Canada) and the MAR was calculated as the interlabel width/labeling period.

Computer-assisted image analysis

After H&E staining or histochemical or immunohistochemical staining of sections from six mice of each genotype, images of fields were photographed with a Sony digital camera. Images of micrographs from single sections were digitally recorded using a rectangular template, and recordings were processed and analyzed using Northern Eclipse image analysis software as described (12,13,21).

Downloaded from https://academic.oup.com/hmg/article/14/11/1515/605493 by guest on 20 April 2024

Statistical analysis

Data from image analysis are presented as mean ± SEM. Statistical comparisons were made using a two-way ANOVA, with $P < 0.05$ being considered significant.

ACKNOWLEDGEMENTS

This work was supported by operating grants to D.M., A.C.K., G.N.H. and D.G. from the Canadian Institutes of Health Research and to D.G. from the National Cancer Institute of Canada.

Conflict of Interest statement. None declared.

REFERENCES

1. Brenza, H.L., Kimmel-Jehan, C., Jehan, F., Shinki, T., Wakino, S., Anazawa, H., Suda, T. and DeLuca, H.F. (1998) Parathyroid hormone activation of the 25-hydroxyvitamin D_3-1alpha-hydroxylase gene promoter. *Proc. Natl Acad. Sci. USA*, **95**, 1387–1391.
2. Murayama, A., Takeyama, K., Kitanaka, S., Kodera, Y., Hosoya, T. and Kato, S. (1998) The promoter of the human 25-hydroxyvitamin D_3-1 alpha-hydroxylase gene confers positive and negative responsiveness to PTH, calcitonin, and 1 alpha,25$(OH)_2D_3$. *Biochem. Biophys. Res. Commun.*, **249**, 11–16.
3. Cantley, L.K., Russell, J., Lettieri, D. and Sherwood, L.M. (1985) 1,25-Dihydroxyvitamin D_3 suppresses parathyroid hormone secretion from bovine parathyroid cells in tissue culture. *Endocrinology*, **117**, 2114–2119.
4. Chan, Y.L., McKay, C., Dye, E. and Slatopolsky, E. (1986) The effect of 1,25 dihydroxycholecalciferol on parathyroid hormone secretion by monolayer cultures of bovine parathyroid cells. *Calcif. Tissue Int.*, **38**, 27–32.
5. Szabo, A., Merke, J., Beier, E., Mall, G. and Ritz, E. (1989) 1,25$(OH)_2$ vitamin D_3 inhibits parathyroid cell proliferation in experimental uremia. *Kidney Int.*, **35**, 1049–1056.
6. Liu, S.M., Koszewski, N., Lupez, M., Malluche, H.H., Olivera, A. and Russell, J. (1996) Characterization of a response element in the 5'-flanking region of the avian (chicken) PTH gene that mediates negative regulation of gene transcription by 1,25-dihydroxyvitamin D_3 and binds the vitamin D_3 receptor. *Mol. Endocrinol*, **10**, 206–215.
7. Beckerman, P. and Silver, J. (1999) Vitamin D and the parathyroid. *Am. J. Med. Sci.*, **317**, 363–369.
8. Arnold, A., Horst, S.A., Gardella, T.J., Baba, H., Levine, M.A. and Kronenberg, H.M. (1990) Mutation of the signal peptide-encoding region of the preproparathyroid hormone gene in familial isolated hypoparathyroidism. *J. Clin. Invest.*, **86**, 1084–1087.
9. Sunthornthepvarakul, T., Churesigaew, S. and Ngowngarmratana, S. (1999) A novel mutation of the signal peptide of the preproparathyroid hormone gene associated with autosomal recessive familial isolated hypoparathyroidism. *J. Clin. Endocrinol. Metab.*, **84**, 3792–3796.
10. Parkinson, D.B. and Thakker, R.V. (1992) A donor splice site mutation in the parathyroid hormone gene is associated with autosomal recessive hypoparathyroidism. *Nat. Genet.*, **1**, 149–152.
11. Kato, S., Yoshizazawa, T., Kitanaka, S., Murayama, A. and Takeyama, K. (2002) Molecular genetics of vitamin D-dependent hereditary rickets. *Hormone Res.*, **57**, 73–78.
12. Miao, D., He, B., Lanske, B., Bai, X.Y., Tong, X.K., Hendy, G.N., Goltzman, D. and Karaplis, A.C. (2004) Skeletal abnormalities in Pth-null mice are influenced by dietary calcium. *Endocrinology*, **145**, 2046–2053.
13. Panda, D.K., Miao, D., Tremblay, M.L., Sirois, J., Farookhi, R., Hendy, G.N. and Goltzman, D. (2001) Targeted ablation of the 25-hydroxyvitamin D 1alpha-hydroxylase enzyme: evidence for skeletal, reproductive, and immune dysfunction. *Proc. Natl Acad. Sci. USA*, **98**, 7498–7503.
14. Dardenne, O., Prud'homme, J., Arabian, A., Glorieux, F.H. and St-Arnaud, R. (2001) Targeted inactivation of the 25-hydroxyvitamin D(3)-1(alpha)-hydroxylase gene (CYP27B1) creates an animal model of pseudovitamin D-deficiency rickets. *Endocrinology*, **142**, 3135–3141.
15. Fraser, D., Kooh, S.W., Kind, H.P., Holick, M.F., Tanaka, Y. and DeLuca, H.F. (1973) Pathogenesis of hereditary vitamin-D-dependent rickets. An inborn error of vitamin D metabolism involving defective conversion of 25-hydroxyvitamin D to 1 alpha,25-dihydroxyvitamin D. *N. Engl. J. Med.*, **289**, 817–822.
16. Eil, C., Liberman, U.A. and Marx, S.J. (1986) The molecular basis for resistance to 1,25-dihydroxyvitamin D: studies in cells cultured from patients with hereditary hypocalcemic 1,25$(OH)_2D_3$-resistant rickets. *Adv. Exp. Med. Biol.*, **196**, 407–422.
17. Zierold, C., Mings, J.A. and DeLuca, H.F. (2003) Regulation of 25-hydroxyvitamin D3-24-hydroxylase mRNA by 1,25-dihydroxyvitamin D_3 and parathyroid hormone. *J. Cell. Biochem.*, **88**, 234–237.
18. Hoenderop, J.G., Dardenne, O., Van Abel, M., Van Der Kemp, A.W., Van Os, C.H., St -Arnaud, R. and Bindels, R.J. (2002) Modulation of renal Ca^{2+} transport protein genes by dietary Ca^{2+} and 1,25-dihydroxyvitamin D_3 in 25-hydroxyvitamin D_3-1alpha-hydroxylase knockout mice. *FASEB J.*, **16**, 1398–1406.
19. Hoenderop, J.G., Nilius, B. and Bindels, R.J. (2005) Calcium absorption across epithelia. *Physiol. Rev.*, **85**, 373–422.
20. Okano, T., Tsugawa, N., Morishita, A. and Kato, S. (2004) Regulation of gene expression of epithelial calcium channels in intestine and kidney of mice by 1alpha,25-dihydroxyvitamin D_3. *J. Steroid. Biochem. Mol. Biol.*, **89–90**, 335–338.
21. Miao, D., He, B., Karaplis, A.C. and Goltzman, D. (2002) Parathyroid hormone is essential for normal fetal bone formation. *J. Clin. Invest.*, **109**, 1173–1182.
22. Lin, R., Amizuka, N., Sasaki, T., Aarts, M.M., Ozawa, H., Goltzman, D., Henderson, J.E. and White, J.H. (2002) 1Alpha,25-dihydroxyvitamin D_3 promotes vascularization of the chondro-osseous junction by stimulating expression of vascular endothelial growth factor and matrix metalloproteinase 9. *J. Bone Miner. Res.*, **17**, 1604–1612.
23. Yoshizawa, T., Handa, Y., Uematsu, Y., Takeda, S., Sekine, K., Yoshihara, Y., Kawakami, T., Arioka, K., Sato, H., Uchiyama, Y. *et al.* (1997) Mice lacking the vitamin D receptor exhibit impaired bone formation, uterine hypoplasia and growth retardation after weaning. *Nat. Genet.*, **16**, 391–396.
24. Erben, R.G., Scutt, A.M., Miao, D., Kollenkirchen, U. and Haberey, M. (1997) Short-term treatment of rats with high dose 1,25-dihydroxyvitamin D_3 stimulates bone formation and increases the number of osteoblast precursor cells in bone marrow. *Endocrinology*, **138**, 4629–4635.
25. Li, Y.C., Pirro, A.E., Amling, M., Delling, G., Baron, R., Bronson, R. and Demay, M.B. (1997) Targeted ablation of the vitamin D receptor: an animal model of vitamin D-dependent rickets type II with alopecia. *Proc. Natl Acad. Sci. USA*, **94**, 9831–9835.
26. Boyan, B.D., Sylvia, V.L., McKinney, N. and Schwartz, Z. (2003) Membrane actions of vitamin D metabolites 1alpha,25$(OH)_2D_3$ and 24R,25$(OH)_2D_3$ are retained in growth plate cartilage cells from vitamin D receptor knockout mice. *J. Cell. Biochem.*, **90**, 1207–1223.
27. Panda, D.K., Miao, D., Bolivar, I., Li, J., Huo, R., Hendy, G.N. and Goltzman, D. (2004) Inactivation of the 25-hydroxyvitamin D 1alpha-hydroxylase and vitamin D receptor demonstrates independent and interdependent effects of calcium and vitamin D on skeletal and mineral homeostasis. *J. Biol. Chem.*, **279**, 16754–16766.
28. Miao, D., Bai, X., Panda, D., McKee, M., Karaplis, A. and Goltzman, D. (2001) Osteomalacia in hyp mice is associated with abnormal phex expression and with altered bone matrix protein expression and deposition. *Endocrinology*, **142**, 926–939.
29. Miao, D., Liu, H., Plut, P., Niu, M., Huo, R., Goltzman, D. and Henderson, J.E. (2004) Impaired endochondral bone development and osteopenia in Gli2-deficient mice. *Exp. Cell. Res.*, **294**, 210–222.
30. Wu, S., Palese, T., Mishra, O.P., Delivoria-Papadopoulos, M. and De Luca, F. (2004) Effects of Ca^{2+} sensing receptor activation in the growth plate. *FASEB J.*, **18**, 143–125.
31. Stern, P.H. (1990) Vitamin D and bone. *Kidney Int. Suppl.*, **29**, S17–S21.
32. Kos, C.H., Karaplis, A.C., Peng, J.B., Hediger, M.A., Goltzman, D., Mohammad, K.S., Guise, T.A. and Pollak, M.R. (2003) The calcium-sensing receptor is required for normal calcium homeostasis independent of parathyroid hormone. *J. Clin. Invest.*, **111**, 1021–1028.
33. Miao, D., Li, J., Xue, Y., Su, H., Karaplis, A.C. and Goltzman, D. (2004) Parathyroid hormone-related peptide is required for increased trabecular bone volume in parathyroid hormone-null mice. *Endocrinology*, **145**, 3554–3562.

Downloaded from https://academic.oup.com/hmg/article/14/11/1515/605493 by guest on 20 April 2024

34. Miao, D., Tong, X.K., Chan, G.K., Panda, D., McPherson, P.S. and Goltzman, D. (2001) Parathyroid hormone-related peptide stimulates osteogenic cell proliferation through protein kinase C activation of the Ras/mitogen-activated protein kinase signaling pathway. *J. Biol. Chem.*, **276**, 32204–32213.
35. Miao, D. and Scutt, A. (2002) Histochemical localization of alkaline phosphatase activity in decalcified bone and cartilage. *J. Histochem. Cytochem.*, **50**, 333–340.
36. He, B., Deckelbaum, R.A., Miao, D., Lipman, M.L., Pollak, M., Goltzman, D. and Karaplis, A.C. (2001) Tissue-specific targeting of the pthrp gene: the generation of mice with floxed alleles. *Endocrinology*, **142**, 2070–2077.
37. Miao, D. and Scutt, A. (2002) Recruitment, augmentation and apoptosis of rat osteoclasts in 1,25-$(OH)_2D_3$ response to short-term treatment with 1,25-dihydroxyvitamin D_3 *in vivo. BMC Musculoskelet. Disord.*, **3**, 16/12052261.

Downloaded from https://academic.oup.com/hmg/article/14/11/1515/605493 by guest on 20 April 2024